Global Journal of Researches in Engineering: A
Mechanical and Mechanics Engineering
Volume 22 Issue 2 Version 1.0 Year 2022
Type: Double Blind Peer Reviewed International Research Journal
Publisher: Global Journals
Online ISSN: 2249-4596 & Print ISSN: 0975-5861

Numerical Analysis and Parametric Optimization of a Static Wavy Flag for Heat Transfer Enhancement

By Swadesh Suman & Sanjay Mahadev Gaikwad
Army Institute of Technology

Abstract- This work investigates the effect of different parameters of a static wavy flag vortex generator on the heat transfer in a rectangular channel using Computational Fluid Dynamics (CFD) analysis. This work encompasses optimizing several parameters of a flag such as flag height from the surface, position in the channel, number of triangular shapes in a flag, and rectangular surface area of the flag. Post analysis results exhibit encouraging results with average Nusselt number in flag height (FH) optimization exceeding that in no flag condition by 41.84%, 47.79%, 54.68% for Re 8236, 12354, and 18344, respectively whereas further position optimization of FH optimized flag exceeds average Nusselt number in no flag condition by 46.86%, 70.68% and 87.26% for the corresponding Re. With significantly less practical application of flags for heat transfer enhancement in industry, this work aims to establish flags as an effective heat transfer enhancement device and demonstrate that with the right optimized parameters, a significant increase of heat transfer in the channel can be achieved.

Keywords: *convective heat transfer, heat transfer enhancement, turbulence, vortex generator.*

GJRE-A Classification: *DDC Code: 621.4022 LCC Code: TJ260*

Strictly as per the compliance and regulations of:

Numerical Analysis and Parametric Optimization of a Static Wavy Flag for Heat Transfer Enhancement

Swadesh Suman [α] & Sanjay Mahadev Gaikwad [σ]

Abstract- This work investigates the effect of different parameters of a static wavy flag vortex generator on the heat transfer in a rectangular channel using Computational Fluid Dynamics (CFD) analysis. This work encompasses optimizing several parameters of a flag such as flag height from the surface, position in the channel, number of triangular shapes in a flag, and rectangular surface area of the flag. Post analysis results exhibit encouraging results with average Nusselt number in flag height (FH) optimization exceeding that in no flag condition by 41.84%, 47.79%, 54.68% for Re 8236, 12354, and 18344, respectively whereas further position optimization of FH optimized flag exceeds average Nusselt number in no flag condition by 46.86%, 70.68% and 87.26% for the corresponding Re. With significantly less practical application of flags for heat transfer enhancement in industry, this work aims to establish flags as an effective heat transfer enhancement device and demonstrate that with the right optimized parameters, a significant increase of heat transfer in the channel can be achieved.

Keywords: convective heat transfer, heat transfer enhancement, turbulence, vortex generator.

I. Introduction

Performance optimization of systems involving heat transfer through channels has always been the area of focus in the past decades. Numerous systems which employ heat transfer through channels like automotive, refrigeration and air-conditioning, electrical and electronic system are becoming compact gradually and with it, the demand for effective and efficient heat transfer is increasing. Correlations presented by Dittus and Boelter well relate the Nusselt number inside the channel with the Reynolds number and the Prandtl number of the fluid [1]. Modification of the Nusselt number is generally attained by altering the Reynolds number as varying the Prandtl number is rather challenging. Alteration of the Reynolds number is accomplished by introducing additional turbulences in the flow. One of the methods employed for introducing additional turbulences in the flow is the utilization of vortex generators.

Author α: Department of Mechanical Engineering, Army Institute of Technology, Pune, India. e-mail: swadesh.ni@gmail.com
Author σ: Assistant Professor, Department of Mechanical Engineering, Army Institute of Technology, Pune, Maharashtra, India.
e-mail: gaikwads.sanjay@gmail.com

Ralph Kristoffer B. Gallegos and Rajnish N Sharma [2] outlined the categories as well as the advantages and disadvantages of each category of vortex generators and presented a brief review on flags as vortex generators. The two categories of vortex generators are active and passive. Many reviews and studies on passive vortex generators like swirl flow devices and other approaches including bubble fin assistance, surface modifications, reduced weight fin configuration, etc. have been extensively reported [3-10]. The use of active vortex generators like piezo fans and magnetic fans for improvement of heat transfer is studied by Gilson GM et al. [11] and Ma HK et al. [12,13]. Jae Bok Lee et al. [14,15] explored the dynamics of the flag in symmetric as well as asymmetric configuration and the effects of various parameters such as bending rigidity, channel height, and Reynolds number on the overall thermal efficiency of the system. Zheng Li et al. [16] studied the effects of Youngs's modulus of the flapping vortex generator on its vorticity fields and heat transfer performances. Atul Kumar Soti et al. [17] used a fluid-structure interaction solver to show the flow-induced deformation as an effective heat transfer technique and examined the role of the Reynolds number, Prandtl number, and the material properties of the plate in the thermal improvement. Jaeha Ryu et al. [18] examined the flapping dynamics of the flag in terms of bending rigidity and Reynold number employing the immersed boundary method. Sung Goon Park et. al [19] with the help of immersed boundary method studied the various dynamic modes of the flag and the vortical structures produced in the wake region of the flag. F. Herrault et al. [20] and Hidalgo and Glezer [21,22] utilized oscillating reeds in the high aspect ratio rectangular microchannels and manifested significant improvements in the thermal performance of the system. Shoele and Mittal [23] studied the material properties of flexible reed on vibratory dynamics, and heat transfer, establishing that thermal performance depends more strongly on the reed inertia than its bending stiffness.

Some recent performance optimization of an engineering system is also based on constructal theory. According to the constructal theory by A. Bejan: "For a finite-size flow system to persist in time (to live) its configuration must change in time so that it provides greater and greater access to its currents" [24]. A review

Nomenclature

ρ_a	Density of fluid (air) (kg/m^3)	T_i	Initial average temperature of the fluid at the channel's inlet (K)
A_c	Cross section area of the channel (m^2)	T_d	Difference between the final and initial average temperature of the fluid (K)
V	Velocity of the fluid (air) (m/s)	T_w	Average temperature of the aluminium plate surface (K)
C_p	Specific heat capacity of air at constant pressure (J/kg K)	T_f	Average temperature of the fluid (K)
k	Thermal Conductivity of the medium (w/m-K)	T_a	Difference between the average temperature of the surface and fluid (K)
μ	Dynamic viscosity of the fluid (air) (Pa.s)	FH	Flag height
ρ_{al}	Density of aluminium (kg/m^3)	RS	Rectangular surface
A_s	Surface area of the aluminium plate (m^2)		FLAG GEOMETRIES
$C_{p(al)}$	Specific heat capacity of aluminium at constant pressure (J/kg K)	ROTF	Rectangular flag combined with one triangular flag
k_{al}	Thermal Conductivity of aluminium (w/m-K)	RTTF	Rectangular flag combined with two triangular flags
Q	Heat carried away by the fluid (w/m^2)	RTeTF	Rectangular flag combined with three triangular flags
D_h	Hydraulic diameter of the channel (m)	RFTF	Rectangular flag combined with four triangular flags
$\dot{M}$	Mass flow rate (kg/s)	RFiTF	Rectangular flag combined with five triangular flags
h	Average heat transfer coefficient (w/m^2 K)		
Nu	Average Nusselt number of the fluid		
Re	Reynolds number		
$\emptyset_q$	Heat flux (W/m^2)		
T	Temperature (K)		
T_o	Final average temperature of the fluid at the channel's outlet (K)		

of constructal theory and the ongoing research trends in this domain is presented by A. Bejan and S. Lorente in [25,26]. Chen LinGen [27,28] focuses on the emergence and expansion of constructal theory and its application in China over the past decade to solve engineering problems. Adrian Bejan [29] solved the fundamental problem of collection and channeling the heat generated volumetrically in a low conductivity volume of a given size to one point. Huijun Feng et al. [30] emphasized enhancing the heat transfer rates by just making a few design changes based on an optimized process of heat and mass transfer between the fluids and used constructal optimization for heat dissipation in "+" shaped high conductivity channels to increase the global heat conductivity performance of electronic device [31] and to reduce entransy dissipation rate of X-shaped vascular networks (XSNV) [32]. Chen LinGen et al. [33] have accomplished optimal constructs of the eight types of heat sinks with different constraints and carried out a comparison between them based on the different optimization objectives. Huijun Feng et al. [34] executed a triple optimization on an irreversible Kalina cycle system 34 (KCS-34) model with variable temperature heat reservoirs using finite-time-thermodynamics. H. J. Feng et al. [35] have adopted a Global optimization method to study the tree-shaped hot network over a rectangular area. Huijun Feng et al. [36] carried out the constructal design of a supercharged boiler (SB) superheater with optimization objectives as heat transfer rate and power consumption factors of SB superheater.

This work builds on the earlier work of Swadesh Suman et al. [37]. According to Swadesh suman et al. [37], the shape exhibiting the highest heat transfer is the

combination of rectangular and two triangular shapes (RTTF). This work utilizes RTTF for the further optimization process. The channel geometry, velocity conditions, boundary conditions, and fluid properties are identical to that used by Swadesh Suman et al. [37]. ANSYS 2014 is used for the numerical work. Geometry is modeled in ANSYS ICEM, analysis, and post-processing is carried out in ANSYS FLUENT and ANSYS CFD-POST, respectively.

II. Problem Description

a) Channel Geometry, Fluid Properties and Boundary Condition

The channel geometry, fluid properties, and boundary conditions are identical to that employed in the investigation carried out by Swadesh suman et al. [37]. The length, breadth, and height of the channel are 150 mm, 150 mm, and 110 mm respectively which set forth the hydraulic diameter of the channel as 126.9 mm. A heater of 20 w capacity, which provides a constant heat flux of 888.88 w/m^2, is installed in the identical fashion as that in the investigation of Swadesh [37]. The existing fluid in the channel is air. The air temperature at the inlet of the channel is between 25 and 30 degrees Celsius so the density, dynamic viscosity, thermal conductivity, and specific heat of air is taken as 1.174 kg/m^3, 18.605 μ Pa.s, 0.0256 w/m-k, 1006.43 j/kg-k respectively. At the channel's inlet velocity inlet boundary condition and at the channel's outlet pressure outlet boundary condition with outlet pressure as 1 atm is applied. No slip boundary condition is employed at the channel's walls and the flag surface. Three different velocity conditions i.e., 1.1 m/s, 1.65 m/s, and 2.45 m/s are used for the numerical investigation.

b) Governing Equations

Since the study involves both heat conduction and convection, it is one of the classical problems of conjugate heat transfer. The conduction in the aluminum plate is a three-dimensional steady state without a heat source within the plate. The equation shows 3-D steady state heat conduction equation without a heat source within the volume [1].

$$\frac{\partial}{\partial x}\left(\frac{\partial T}{\partial x}\right)+\frac{\partial}{\partial y}\left(\frac{\partial T}{\partial y}\right)+\frac{\partial}{\partial z}\left(\frac{\partial T}{\partial z}\right)=0 \quad (1)$$

Where T is the temperature.

Standard K - **ε** viscous model is used in Ansys Fluent for the analysis as the Reynolds number falls under the turbulent range. The standard K - **ε** model requires two additional equations to solve the additional unknown given by the Reynolds stress term in the RANS equation (Reynolds Average Navier Stokes) [38].

$$\rho\bar{u}_j\frac{\partial\bar{u}_i}{\partial x_j}=\rho\bar{f}_i+\frac{\partial}{\partial x_j}[-\bar{p}\delta_{ij}+\mu(\frac{\partial\bar{u}_i}{\partial x_j}+\frac{\partial\bar{u}_j}{\partial x_i})-\rho\overline{u'_i u'_j}] \quad (2)$$

Here,

u represents instantaneous velocity

$\bar{u}$ represents mean (time averaged) component of velocity

u' represents fluctuating component of velocity

ρ represents density

$\overline{f_i}$ is a vector representing external forces

μ represents dynamic viscosity of fluid

The additional equations of K - **ε** model are [32]

For turbulent kinetic energy K

$$\frac{\partial}{\partial t}(\rho k)+\frac{\partial}{\partial x_i}(\rho k u_i)=\frac{\partial}{\partial x_j}\left[\frac{\mu_t}{\sigma_k}\frac{\partial k}{\partial x_j}\right]+2\mu_t E_{ij}E_{ij}+\rho\epsilon \quad (3)$$

For dissipation Rate **ε**

$$\frac{\partial}{\partial t}(\rho\epsilon)+\frac{\partial}{\partial x_i}(\rho k u_i)=\frac{\partial}{\partial x_j}[u\frac{\mu_t}{\sigma_\epsilon})\frac{\partial\epsilon}{\partial x_j}]+C_{1\epsilon}\frac{\epsilon}{k}2\mu_t E_{ij}E_{ij}-C_{2\epsilon}\rho\frac{\epsilon^2}{k} \quad (4)$$

u_i represents velocity component in corresponding direction

E_{ij} represents component of rate of deformation

μ_t represent eddy viscosity

$$\mu_t=\rho C_\mu\frac{k^2}{\epsilon}$$

The equations also consist of some adjustable constants σ_k, σ_ϵ,$C_{1\epsilon}$,$C_\mu$and $C_{2\epsilon}$. The values of these constants have been arrived at by numerous iterations of data fitting for a wide range of turbulent flows [39]. These are as follows:

$\sigma_k = 1.00$
$\sigma_\epsilon = 1.30$
$C_\mu = 0.09$
$C_{1\epsilon} = 1.44$
$C_{2\epsilon} = 1.92$

c) Selection of Parameters

Various parameters related to the flag are the shape of the flag, the position of the flag in the channel, the height of the flag from the surface, the surface area of the flag, and the width of the flag. For the optimization based on the shape of a flag, the shape optimized flag established by Swadesh suman et al. [37] is selected. Two other parameters which can be selected from the shape optimized flag is the number of triangular shape and the relative area of the rectangular shape of the flag. This shape-optimized flag is used for further parametric optimization. Keeping the width of the flag constant, the various parameters to optimize are the height of the flag

from the surface, the position of the flag in the channel, the number of triangular shapes, and the relative area of the rectangular shape in the shape-optimized flag.

d) Grid Independence Study

To remove the influence of the grid size on the result, a grid independence study is performed by varying the Grade scale factor (GSF) of the meshing in Ansys ICEM. The geometry selected is the rectangular channel with no flag condition. The initial value of GSF is kept at 1 and was increased by 0.5 until the variation of the *Nu* is acceptable. The Reynolds number for this study is chosen as 12354 corresponding to the velocity of 1.65 m/s. Table 1 shows the total number of cells, nodes, and *Nu* variation at different values of GSF.

Table 1: Variation of *Nu* with GSF

GSF	Total number of cells	Total number of nodes	*Nu*	*Re*
1	302502	54225	256.7	12354
1.5	1025087	180077	247.4	12354
2	2430221	419890	249.2	12354
2.5	4709977	806414	247.7	12354
3	8193797	1398852	240.5	12354

The *Nu* value at GSF 1.5 showed a drop of 3.62% than the *Nu* value at GSF 1. Although this drop is within the permissible limit, to further reduce the error analysis is carried out at GSF 2. At GSF 2 the variation in the *Nu* value was just 0.72%. Further at GSF 2.5 and 3, it showed the variation of 0.61% and 2.9% respectively. So, based on the variation at different GSF values and time of computation, the ideal value of GSF is chosen 2 and further analysis is carried out at GSF 2.

III. Flag Height (FH) Optimization

a) Representation of FH and CFD Simulations

Figure 1 represents flag height (FH) which is varied to find the optimum height of RTTF from the plate. Shape-optimized RTTF and its arrangement in the channel by Swadesh Suman et al. [37] is used for FH optimization. The initial height of RTTF from the plate is 2.5 mm. FH is varied from 0.5 mm to 5 mm, increasing it by 0.5 mm from 0.5 mm to 3 mm and by 1 mm from 3 mm to 5 mm.

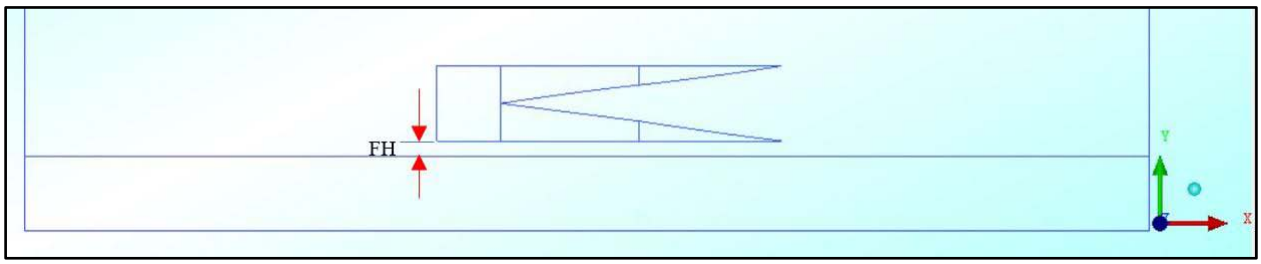

Figure 1: Representation of Flag Height (FH)

Figure 2a and 2b show the thermal boundary layer formed in the case of FH 1 mm and FH 2 mm. The temperature contour in each case shows the difference in temperature.

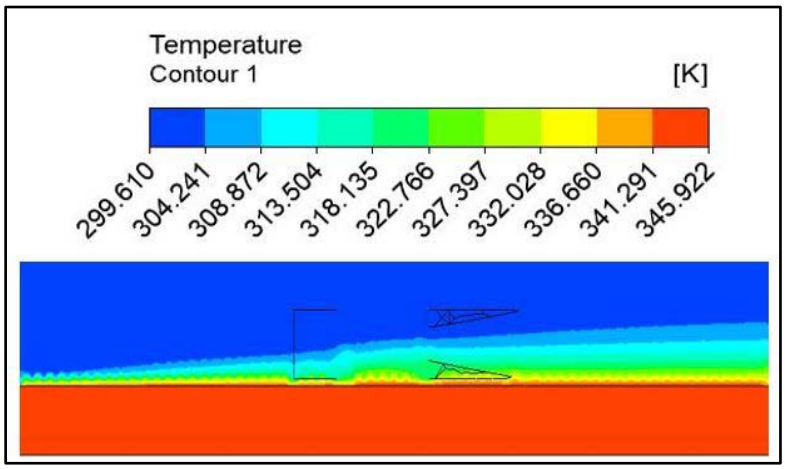

Figure 2a): FH = 1 mm

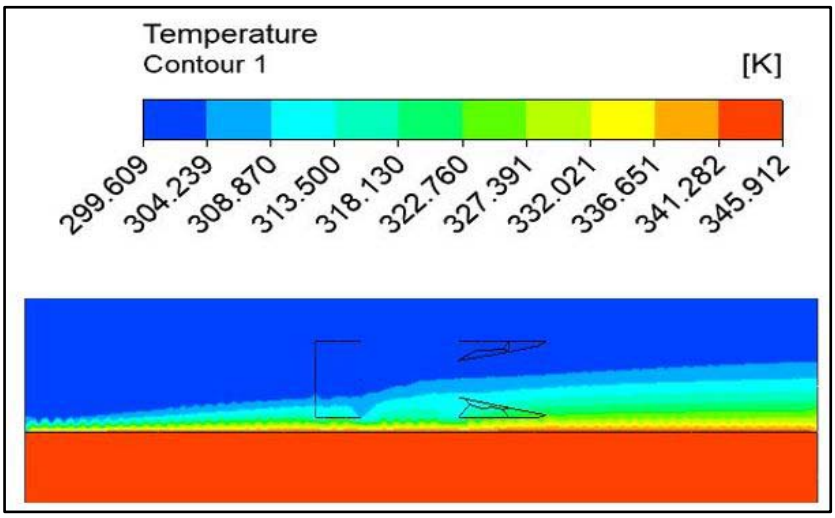

Figure 2b): FH = 2 mm

Figure 2: Thermal Boundary Layer at Different Flag Height

b) Procedure followed during Calculations

The procedure followed during the calculations is same as that used by Swadesh Suman et al. [37]. Fig 3 shows the lines plotted along the length of the channel and an average temperature is obtained for each line. The well distributed lines along the channel's height gives good idea of the average temperature of air at channel's outlet.

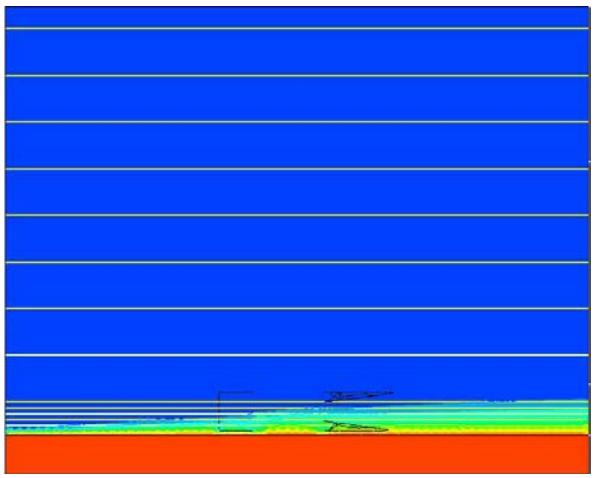

Figure 3: Lines Plotted along the Length of the Channel

Following procedure is then followed to find out the average Nusselt number in each case:-

Step 1: Mass flow rate $(\dot{M}) = \rho \times A_c \times V$ (5)

Step 2: Temperature change in fluid $(T_d) = T_o - T_i$ (6)

Step 3: Heat carried away by the fluid $(Q) = \dot{M} \times C_p \times T_d$ (7)

Step 4: Average temperature difference between surface and fluid $(T_a) = T_w - T_f$ (8)

Step 5: Average heat transfer coefficient $(h) = \frac{Q}{A_s \times T_a}$ (9)

Step 6: Nusselt no $(Nu) = \frac{h \times D_h}{k}$ (10)

Step 7: Reynolds no $(Re) = \frac{\rho \times V \times D_h}{\mu}$ (11)

c) Results and Discussion

Table 2 shows the Nusselt number for each flag height at different velocity conditions. The highest *Nu* is achieved at a flag height equal to 1 mm for each velocity condition and it increases significantly by 10.06%, 7.28%, and 7.55% when compared with *Nu* values for flag height of 1.5 mm and exceeds that in no flag condition by 41.84%, 47.79%, 54.68% for Re 8236, 12354 and 18344, respectively. *Nu* values at each different velocity condition shoot up with the decrease in

FH up to 1 mm. At FH 0.5 mm, *Nu* values diminishes significantly by 11.1%, 9.3%, and 8.5% than that of FH 1 mm for *Re* 8236, 12354, and 18344, respectively. The same has been depicted in fig 4 which presents the graph between *Nu* and *Re*.

Table 2: Nusselt Number at Different Flag Heights

Velocity (m/s)	*Nu*	*Re*
No flag condition		
1.1	239	8236
1.65	249	12354
2.45	267	18344
FH 0.5 mm		
1.1	301	8236
1.65	334	12354
2.45	380	18344
FH 1 mm		
1.1	339	8236
1.65	368	12354
2.45	413	18344
FH 1.5 mm		
1.1	308	8236
1.65	343	12354
2.45	384	18344
FH 2 mm		
1.1	299	8236
1.65	312	12354
2.45	348	18344
FH 2.5 mm		
1.1	288	8236
1.65	301	12354
2.45	324	18344
FH 3 mm		
1.1	278	8236
1.65	294	12354
2.45	322	18344
FH 4 mm		
1.1	274	8236
1.65	291	12354
2.45	319	18344
FH 5 mm		
1.1	272	8236
1.65	287	12354
2.45	314	18344

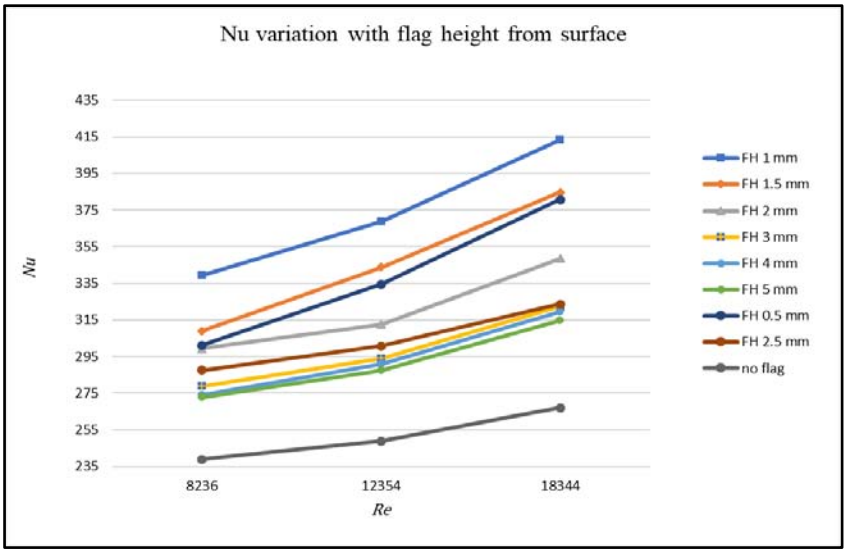

Figure 4: Average Nusselt Number vs Reynolds Number for Different Flag Heights

IV. Optimization of Position of Flag in Channel

a) Representation of Position of the Flag

RTTF with FH 1 mm is used for the optimization of the position of the flag. Figure 5 represents the position of the flag from the inlet which is varied to find the optimum position of RTTF from the inlet. The initial position of RTTF from the inlet is 55 mm. The position from the inlet is varied from 15 mm to 65 mm, increasing it by 10 mm in each step.

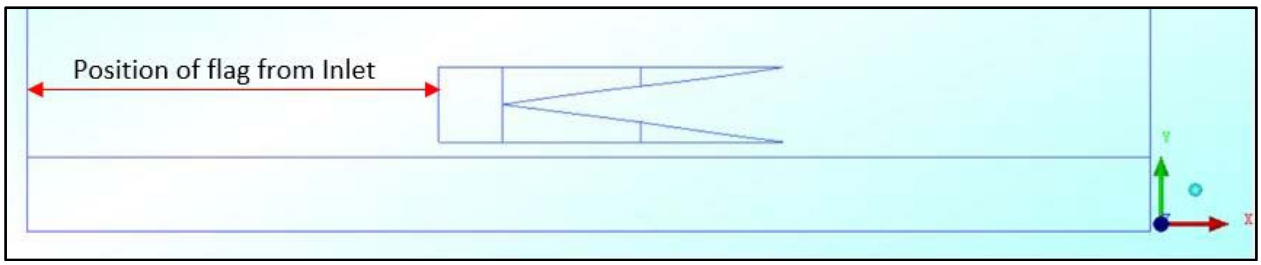

Figure 5: Representation of Position of Flag from inlet

b) Procedure followed during Calculations

The procedure followed for the calculation of *Nu* is the same as that of Flag height optimization.

c) Results and Discussion

Table 3 shows the Nusselt number for the position of the flag at different velocity conditions. The highest *Nu* is achieved at a flag position equal to 35 mm for each velocity condition. *Nu* at flag position 35 mm is greater than that at flag position 25 mm by 2.63%, 6.78%, 10.13%, and by 2.03%, 8.97%, 12.10% for *Re* 8236, 12354, 18344 respectively when compared with *Nu* values for flag position 45 mm. Whereas it exceeds *Nu* in no flag condition by 46.86%, 70.68%, and 87.26% for the corresponding Re. In each case, the percentage rise in *Nu* increases with an increase in the velocity of air in the channel. *Nu* values at each different velocity condition shoot up with the decrease in flag positions from 65 mm up to 35 mm and afterward, it diminishes till the flag position is 15 mm. The same has been depicted in fig 6 which presents the graph between *Nu* and *Re*.

Table 3: Nusselt number at different flag positions

Velocity (m/s)	*Nu*	*Re*
No flag condition		
1.1	239	8236
1.65	249	12354
2.45	267	18344
Position of flag = 15 mm		

1.1	340	8236
1.65	372	12354
2.45	438	18344
Position of flag = 25 mm		
1.1	342	8236
1.65	398	12354
2.45	454	18344
Position of flag = 35 mm		
1.1	351	8236
1.65	425	12354
2.45	500	18344
Position of flag = 45 mm		
1.1	344	8236
1.65	390	12354
2.45	446	18344
Position of flag = 55 mm		
1.1	339	8236
1.65	368	12354
2.45	413	18344
Position of flag = 65 mm		
1.1	268	8236
1.65	295	12354
2.45	319	18344

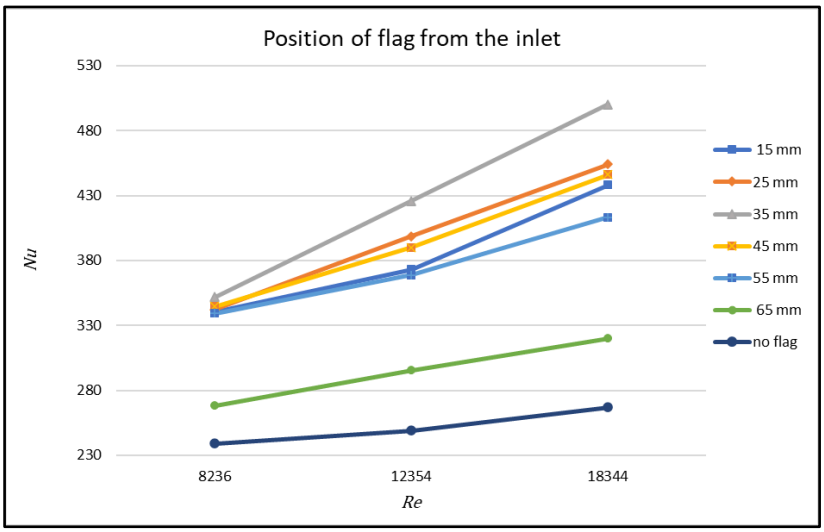

Figure 6: Average Nusselt number vs Reynolds number for different position of flag

V. Optimization of Number of Triangular Shape in RTTF

a) Flag Geometries

RTTF used for this stage has FH as 1 mm and position from the inlet as 35 mm. In the investigation by Swadesh suman et al. [37], RTTF showed higher heat transfer than ROTF. So, to check the dependency of heat transfer on the number of triangular shapes, the number of triangular shapes is varied. Fig. 7 shows all five flag geometries. The total surface area of the triangular part of RTTF is kept constant while varying the number of triangular shapes. Fig 7 also incorporates the symbolic representation allotted to each flag with the different number of triangular shapes.

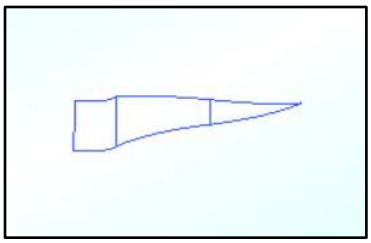

7a) Rectangular flag combined with one triangular flag (ROTF)

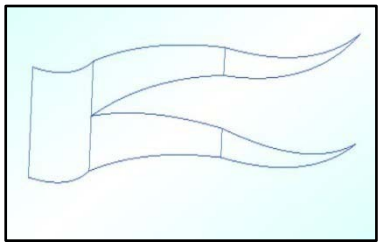

7b) Rectangular flag combined with two triangular flags (RTTF)

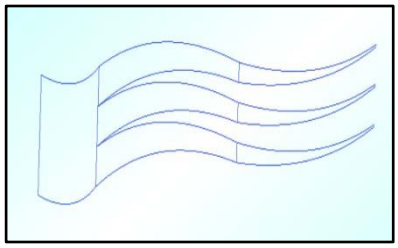

7c) Rectangular flag combined with three triangular flags (RTeTF)

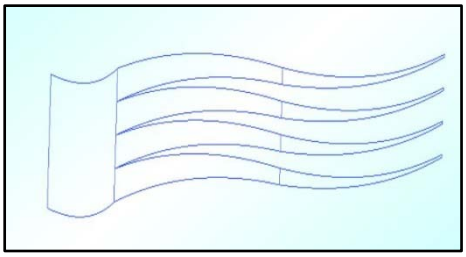

7d) Rectangular flag combined with four triangular flag (RFTF)

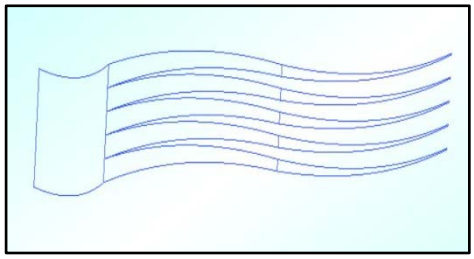

7e) Rectangular flag combined with five triangular flag (RFiTF)

Figure 7: Flag geometries

b) Procedure followed during Calculations

The procedure followed for the calculation of *Nu* is the same as that of Flag height optimization.

c) Results and Discussion

Table 4 shows the Nusselt number for flags with different triangular shapes at different velocity conditions. The highest *Nu* is achieved for RTTF at each velocity condition. *Nu* for RTTF is greater than RFiTF by 6.04%, 17.40%, 26.58% for *Re* 8236, 12354, 18344 respectively and by 8.33%, 18.71%, 31.57% for *Re* 8236, 12354, 18344 respectively when compared with *Nu* values for RFTF. The percentage rise in *Nu* of RTTF increases with an increase in velocity when compared to other flags. Fig 8 shows the graph between *Nu* and *Re* for each distinct flag.

Table 4: Nusselt Number for Flags with Different Number of Triangular shapes

Velocity (m/s)	*Nu*	*Re*
No flag condition		
1.1	239	8236
1.65	249	12354
2.45	267	18344
ROTF		
1.1	285	8236
1.65	308	12354
2.45	345	18344
RTTF		
1.1	351	8236
1.65	425	12354
2.45	500	18344
RTeTF		
1.1	281	8236
1.65	302	12354
2.45	341	18344

RFTF		
1.1	324	8236
1.65	358	12354
2.45	380	18344
RFiTF		
1.1	331	8236
1.65	362	12354
2.45	395	18344

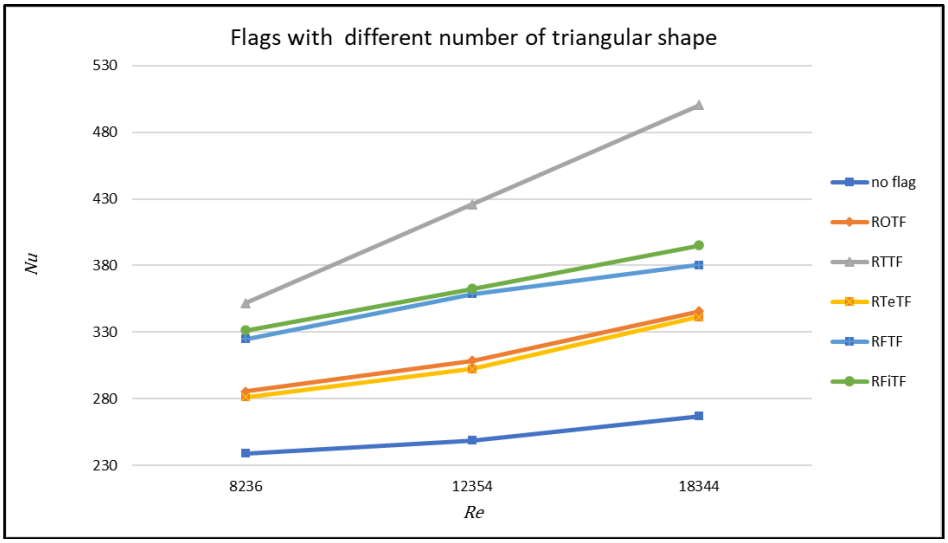

Figure 8: Average Nusselt number vs Reynolds number for different number of triangular shapes

VI. Optimization of the Rectangular Surface (RS) Area of Flag

a) *Problem Description*

RTTF has the highest heat transfer during the optimization process based on the number of triangular shapes. So, for the rectangular surface area optimization, RTTF is chosen. The surface area of the rectangular part in RTTF is 100 mm^2. This area is varied from 50 mm^2 to 150 mm^2 with a step of 25 mm^2.

b) *Procedure followed during Calculations*

The procedure followed for the calculation of *Nu* is the same as that of Flag height optimization.

c) *Results and Discussion*

Table 5 shows the Nusselt number for flags with different RS areas at distinct velocity conditions. The highest *Nu* is achieved for RTTF with RS area of 100 mm^2 at each velocity condition. *Nu* for RTTF with 100 mm^2 is greater than that with 125 mm^2 by 5.72%, 5.19%, 5.48% and that with150 mm^2 by 6.04%, 7.86%, 10.86% for *Re* 8236, 12354, 18344, respectively. Fig 9 shows the graph between *Nu* and *Re* for each distinct flag. Following fig 9, there is an increase in the *Nu* with the increase in RS area from 50 mm^2 to 100 mm^2. At the RS area of 100 mm^2, *Nu* is the highest and afterward, it diminishes with an increase in RS area from 100 mm^2 to 150 mm^2.

Table 5: Nusselt Number for Flags with Different Rectangular Area

Velocity (m/s)	*Nu*	*Re*
No flag condition		
1.1	239	8236
1.65	249	12354
2.45	267	18344
RS area = 50 mm²		
1.1	309	8236
1.65	352	12354
2.45	395	18344

RS area = 75 mm²		
1.1	312	8236
1.65	356	12354
2.45	413	18344
RS area = 100 mm²		
1.1	351	8236
1.65	425	12354
2.45	500	18344
RS area = 125 mm²		
1.1	332	8236
1.65	404	12354
2.45	474	18344
RS area = 150 mm²		
1.1	331	8236
1.65	394	12354
2.45	451	18344

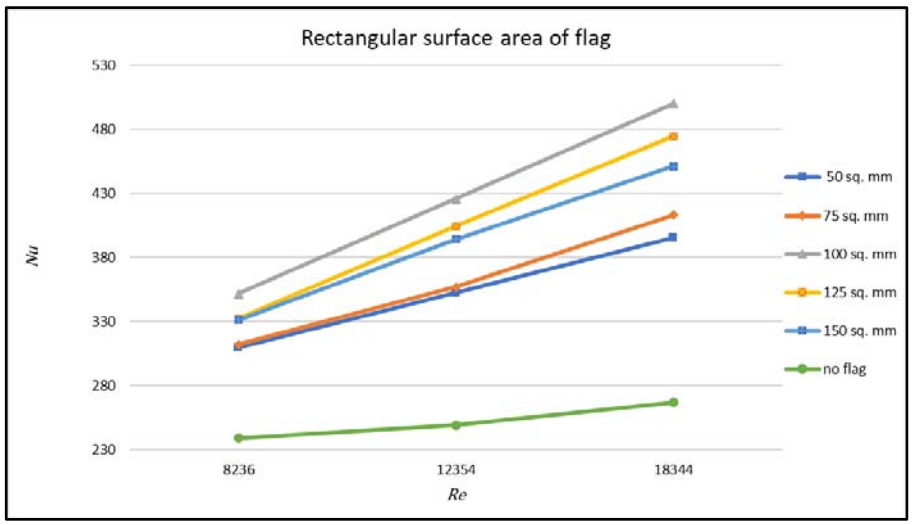

Figure 9: Average Nusselt Number vs Reynolds Number for Different Rectangular Surface Area of Flag

VII. Optimal Parameter Selection and Performance Oprimization

This study is the extension of the investigation carried out by Swadesh Suman et al, [37]. RTTF which is the shape optimized flag according to Swadesh [37] is chosen for the optimization based on new parameters. RTTF's position in the channel is 55 mm from the channel inlet and 2.5 mm from the surface. The position of the flag in the channel and flag height is chosen as the optimization parameters. Since RTTF is the combination of rectangular and two triangular shapes, therefore two other parameters namely the area of the rectangular part and the number of triangular shapes are also chosen as the optimization parameters. Similar to the method adopted by Swadesh [37], the overall optimization process is divided into four stages. For the first stage, RTTF of the shape optimization by Swadesh is considered and for the next stages, the optimized flag from the previous stage is considered.

Table 6 shows the value of *Nu* after each stage of parametric optimization. The % increase in *Nu* in each case shoots up with the increase in the velocity of air in the channel. This can be seen in column 4 of Table 6. The highest increase in *Nu* is observed during the optimization of the position of the flag in the channel.

Table 6: Performance Optimization

Performance optimization			
Velocity (m/s)	*Nu*	*Re*	% Increase in *Nu* wrt no flag
No flag condition			
1.1	239	8236	0
1.65	249	12354	0
2.45	267	18344	0
RTTF from Shape optimization (Swadesh [37])			
1.1	288	8236	20.50
1.65	301	12354	20.88
2.45	324	18344	21.35
After Flag height optimization			
1.1	339	8236	41.84
1.65	368	12354	47.79
2.45	413	18344	54.68
After Optimization of position of flag			
1.1	351	8236	46.86
1.65	425	12354	70.68
2.45	500	18344	87.26
After Optimization of number of triangular shapes			
1.1	351	8236	46.86
1.65	425	12354	70.68
2.45	500	18344	87.26
After Optimization of RS area			
1.1	351	8236	46.86
1.65	425	12354	70.68
2.45	500	18344	87.26

VIII. Conclusion

This present numerical investigation focuses on the effect of different parameters of a static wavy flag vortex generator on heat transfer. These parameters are flag height from the surface, position in the channel, number of triangular shapes in a flag, and rectangular surface area of the flag. The method adopted for numerical investigation is Computational Fluid Dynamics (CFD) and the software used is ANSYS 2014.The ideal value of GSF for the geometry is selected as 2. The overall optimization process is divided into four stages with the first stage being the flag height optimization, the second stage is the position in the channel, the third stage is the number of triangular shapes and the fourth stage is the rectangular surface area of the flag. For each stage, the optimized flag from the previous stage is considered and for the first stage, shape optimized RTTF by Swadesh suman et al. [37] is considered. For the first stage, the highest *Nu* is achieved at flag height equal to 1 mm for each velocity condition exceeding that in no flag condition by 41.84%, 47.79%, 54.68% for Re 8236, 12354, and 18344, respectively. For the decrease in FH from 5 mm to 1 mm, *Nu* values showed an upward trend but with a further decrease in FH to 0.5 mm it diminished. For the second stage, the highest *Nu* is achieved at the flag position equal to 35 mm and it exceeds that in no flag condition by 46.86%, 70.68%, and 87.26% for *Re* 8236, 12354, 18344, respectively. A similar trend as the first stage in *Nu* values is seen in the second one as well, it shoots up with the decrease in flag positions from 65 mm up to 35 mm and then decreases flag position to 15 mm. In the third stage, RTTF with a flag height of 1mm and flag position of 35 mm from the inlet has the highest *Nu* when compared with flags with a different number of triangular shapes. For the fourth and final stage, RTTF with a rectangular area of 100 mm^2 has the highest *Nu* among the flags with the different rectangular areas. The *Nu* increases with the increase in RS area from 50 mm^2 to 100 mm^2 and afterward, it diminishes with an increase in RS area from 100 mm^2 to 150 mm^2. Thus, from the results of this investigation, it can be deduced that with the right

optimized parameters, a significant increase in heat transfer in the channel can be achieved.

References Références Referencias

1. Bergman TL, Incropera FP. Fundamentals of heat and mass transfer, 7. Hoboken, N.J: John Wiley; 2011.
2. Ralph Kristoffer B. Gallegos, Rajnish N Sharma, "Flags as vortex generators for heat transfer enhancement: Gaps and challenges," in *Renewable and Sustainable energy reviews*, 76(2017) 950-962.
3. Sheikholeslami M, Gorji-Bandpy M, Ganji DD. Review of heat transfer enhancement methods: focus on passive methods using swirflow devices. Renew Sustain Energy Rev 2015; 49:444–69.
4. Ahmed HE, Mohammed HA, Yusoff MZ. An overview on heat transfer augmentation using vortex generators and nanofluids: approaches and applications. Renew Sustain Energy Rev 2012; 16:5951–93.
5. Alam T, Saini RP, Saini JS. Use of turbulators for heat transfer augmentation in an air duct – A review. Renew Energy 2014; 62:689–715.
6. Amar Raj Singh Suri, Anil Kumar & Rajesh Maithani (2017), "Convective Heat Transfer Enhancement Techniques of Heat Exchanger Tubes: A Review", in *International Journal of Ambient Energy*, DOI: 10.1080/01430750.2017.1324816.
7. M. Arulprakasajothi, U. Chandrasekhar, K. Elangovan & D. Yuvarajan, "Influence of conical strip inserts in heat transfer enhancement under transition flow", in *International Journal of Ambient Energy*, Volume 41, 2020 - DOI: 10.1080/01430750.2018.1472651.
8. M. Abeens, M. Meikandan, Jaffar Sheriff & R. Murunganadhan, "Experimental analysis of convective heat transfer on tubes using twisted tape inserts, louvered strip inserts and surface treated tube", in *International Journal of Ambient Energy,* Volume 41, 2020- DOI: 10.1080/01430750.2018.1476263.
9. K. Logesh, R. Arunraj, S. Govindan, M. Thangaraj & G. K. Yuvashree, "Numerical investigation on possibility of heat transfer enhancement using reduced weight fin configuration", in *International Journal of Ambient Energy,* Volume 41, 2020 - DOI: 10.1080/01430750.2018.1451382.
10. K. Subramani, K. Logesh, S. Kolappan & S. Karthik, "Experimental investigation on heat transfer characteristics of heat exchanger with bubble fin assistance", in *International Journal of Ambient Energy,* Volume 41, 2020- DOI: 10.1080/01430750.2018.1472654.
11. Gilson GM, Pickering SJ, Hann DB, Gerada C. Piezoelectric fan cooling: a novel high reliability electric machine thermal management solution. Ind Electron IEEE Trans 2013; 60:4841–51.
12. Ma HK, Liao SK, Li YT. Study of multiple magnetic vibrating fins with a piezoelectric actuator. Therm. Meas. Model. Manag. Symp. (SEMI-THERM), 2015 31st, IEEE, 2015, p. 309–13.
13. Ma HK, Tan LK, Li YT. Investigation of a multiple piezoelectric–magnetic fan system embedded in a heat sink. Int Commun Heat Mass Transf 2014; 59:166–73.
14. Jae Bok Lee, Sung Goon Park, Boyoung Kim, Jaeha Ryu, Hyung Jin Sung, "Heat transfer enhancement by flexible flags clamped vertically in a Poiseuille channel flow," in *International Journal of Heat and Mass Transfer,*107 (2017) 391–402.
15. Jae Bok Lee, Sung Goon Park, Hyung JinSung, "Heat transfer enhancement by asymmetrically clamped flexible flags clamped in a channel flow," in *International Journal of Heat and Mass Transfer,*116(2018) 1003-1015.
16. Zheng Li, Xianchen Xu, Kuojiang Li, Yangyang Chen, Guoliang, Huang , Chung-lung Chen, Chien-Hua Chen, "A flapping vortex generator for heat transfer enhancement in a rectangular airside fin,'' in *International Journal of Heat and Mass Transfer,*118 (2018) 1340–1356.
17. Atul Kumar Soti, Rajneesh Bhardwaj, John Sheridan, "Flow-induced deformation of a flexible thin structure as manifestation of heat transfer enhancement" in *International Journal of Heat and Mass Transfer,* 84 (2015) 1070–1081.
18. Jaeha Ryu, Sung Goon Park, Boyoung Kim, Hyung JinSung, "Flapping dynamics of an inverted flag in a uniform flow", in *Journal of fluid and structures* 57 (2015) 159-169.
19. Sung Goon Park, Boyoung Kim, Cheong Bong Chang, Jaeha Ryu, Hyung Jin Sung , "Enhancement of heat transfer by a self-oscillating inverted flag in a Poiseuille channel flow" in *International Journal of Heat and Mass Transfer,* 96 (2016) 360–370.
20. Herrault F, Hidalgo PA, Ji C-H, Glezer A, Allen MG, "Cooling performance of micromachined self-oscillating reed actuators in heat transfer channels with integrated diagnostics", in *Micro Electro Mech. Syst. (MEMS), 2012 IEEE In: Proceedings of the 25th International Conference, IEEE,* 2012, p. 1217–20.
21. Hidalgo P, Glezer A, "Direct actuation of small-scale motions for enhanced heat transfer in heated channels", in *ASME-JSME-KSME 2011 Jt. Fluids Eng. Conference, American Society of Mechanical Engineers,* 2011, p. 3123–9.
22. Hidalgo P, Glezer A, "Small-scale vorticity induced by a self-oscillating fluttering reed for heat transfer augmentation in air cooled heat sinks", in Inter PACK/*ICNMM2015, San Francisco, CA.* 2015.
23. Shoele K, Mittal R, "Computational study of flow-induced vibration of a reed in a channel and effect

on convective heat transfer", in *Phys Fluids* 2014;26:127103.
24. A. Bejan, Advanced Engineering Thermodynamics, 2nd edn, Wiley, New York, 1997.
25. A. Bejan, S. Lorente, "Design with Constructal Theory" New Jersey: Wiley, 2008.
26. Sylvie Lorente, Adrian Bejan, "Current trends in constructal law and evolutionary design" in *Heat Transfer-Asian Research*, 2019, 48(8): 357-389.
27. Chen LinGen, "Progress in study on constructal theory and its applications", in *Science China Technological Sciences* 2012, 10.1007/s11431-011-4701-9.
28. Lingen Chen, Huijun Feng, Zhihui Xie, Fengrui Sun, "Progress of constructal theory in China over the past decade", in *International Journal of Heat and Mass Transfer,* 130 (2019) 393-413.
29. Adrian Bejan, "Constructal-theory network of conducting paths for cooling a heat generating volume", in *International Journal of Heat and Mass Transfer,*0017 9310/97 S17.00- 0.00.
30. Huijun Feng, Lingen Chen, ZhihuiXie, "Multi-disciplinary, multi-objective and multi-scale constructal optimizations for heat and mass transfer processes performed in Naval University of Engineering, a review", in *International Journal of Heat and Mass Transfer*, 115 (2017) 86-98.
31. Huijun Feng, Lingen Chen, ZhihuiXie, "Constructal optimizations for ''+" shaped high conductivity channels based on entransy dissipation rate minimization", in *International Journal of Heat and Mass Transfer*, 119 (2018) 640-646.
32. Feng Huijun, Chen LinGen, XIE Zhihui, "Constructal entransy dissipation rate minimization for X-shaped vascular networks", in *Science China Technological Science*, 11431-018-9392-1.
33. Chen LinGen, Yang AiBo, Feng HuiJun, Ge YanLin, Xia ShaoJun, "Constructal design progress for eight types of heat sinks", in *Science China Technological Science*, 11431-019-1469-1.
34. Huijun Feng, Wanxu Qin, Lingen Chen, Cunguang Cai, Yanlin Gea, Shaojun Xia, "Power output, thermal efficiency and exergy-based ecological performance optimizations of an irreversible KCS-34 coupled to variable temperature heat reservoirs" in *Energy Conversation and Management*, 205 (2020) - 112424.
35. H.J. Feng, L.G. Chen, Z.H. Xie, F.R. Sun, "Constructal complex-objective optimization for tree-shaped hot water networks over a rectangular area using global optimization method", in *International Communications of Heat and Mass Transfer*, 87 (2017) 147-156.
36. Huijun Feng, ZhuojunXie, Lingen Chen, Zhixiang Wu, Shaojun Xia, "Constructal design for supercharged boiler superheater", in *Energy*, 2020, 191: 116484.
37. Swadesh suman, Vineeth Uppada, Swati Singh, Sanjay Mahadev Gaikwad, "Numerical investigation and experimental validation of Shape amd Position optimization of a static wavy flag for heat transfer enhancement", in *International Journal of Ambient Energy,* DOI: 10.1080/01430750.2020.1818120.
38. Hinze, J O., 1975, *Turbulence*, McGraw-Hill, New York.
39. Launder. B. E., Spalding D. B., 1974, "The Numerical Computation of Turbulent Flows," in *Computer Methods in Applied Mechanics and Engineering*, 3, pp. 269–289.